

# LHC explores what LEP hinted at: $CP$ -violating type-I 2HDM

Wolfgang Mader, Jae-hyeon Park, Giovanni Marco Pruna,  
Dominik Stöckinger, and Arno Straessner

*Institut für Kern- und Teilchenphysik, TU Dresden, 01069 Dresden, Germany*

## Abstract

The Large Hadron Collider is shown to have great scope for a light charged Higgs discovery, in the context of the  $CP$ -violating type-I two Higgs doublet model. This scenario with similar masses of  $H^\pm$  and  $W$  was suggested by the puzzling departure from charged current lepton universality found in the LEP data. With the lightest neutral Higgs mass set to 125 GeV, the charged-neutral Higgs associated production mechanism can cause a significant excess in the  $\tau\nu b\bar{b}$  events over a vast range of  $\tan\beta$  as long as the Higgs mixing pattern avoids a few limiting cases. Thanks to the low  $H^\pm$  mass, the charged Higgs loop can play a striking role in neutral Higgs decays into  $\gamma\gamma$ , thereby compensating for a suppressed gluon-gluon fusion rate. The effect of scalar–pseudo-scalar mixing on loop-induced Higgs signals is also discussed.

## I. INTRODUCTION

There are many motivations to introduce an extended Higgs sector. Examples are, including obsolete ones, fine-tuning in the weak-scale Higgs mass [1] suggesting supersymmetry [2],  $CP$ -violation [3, 4], grand unification [5], extended gauge symmetry [6], strong  $CP$  problem [7], string theory [8], vacuum stability [9], light fermion mass/weak-scale hierarchy [10], fermion flavour structure [11], neutrino mass [12], dark matter (see e.g. [13, 14]), cosmic rays [15], baryogenesis [16], inflation [17], novel collider phenomenology [18], as well as anomalies seen in precision (see e.g. [19, 20]) and accelerator (see e.g. [21, 22]) experiments. In this article, we entertain the possibility that an intriguing outcome from the LEP experiment is in fact pointing to an extended Higgs sector, which may be directly inspected at the Large Hadron Collider (LHC).

Specifically, we take as our framework the two Higgs doublet model (2HDM) of type-I with  $M_{H^\pm}$  in the vicinity of the  $W$ -boson mass. The two main points of this paper are the following. (1) The charged Higgs produced in association with the lightest neutral Higgs can be discovered as an excess in the  $pp \rightarrow \tau\nu b\bar{b}$  process at the LHC. Moreover, this could happen even at the early stage with  $\sqrt{s} = 7\text{--}8$  TeV in a substantial portion of the parameter space. (2) With the lightest neutral Higgs mass assumed to be  $\sim 125$  GeV, the charged Higgs one-loop effect can enhance  $\mathcal{B}(H_1 \rightarrow \gamma\gamma)$  enough to produce the excess observed at the recent LHC analyses [23–26]. This enhancement is particularly welcome since the  $H_1$  production at hadron colliders is generically suppressed due to Higgs mixing.

This light charged Higgs scenario was previously advocated in [21], whose contents we recap here. The LEP Electroweak Working Group has performed an analysis of  $W$  decay branching ratios. In their report,  $\mathcal{B}(W \rightarrow \tau\nu)$  appears to be higher than  $\mathcal{B}(W \rightarrow e\nu)$  and  $\mathcal{B}(W \rightarrow \mu\nu)$ , to the level of 2.8 standard deviations [27]. Should this difference be real, it would violate the charged current lepton universality, that is predicted by the gauge invariance of the Standard Model (SM) and has been confirmed in many indirect tests.

As a resolution of this puzzle, one of the authors pointed out that a significant portion of the apparent lepton non-universality can be attributed to production of light charged Higgs pairs which predominantly decay to the  $\tau\nu$  final states [21]. One of the most natural ways to realise a  $H^\pm$  that has mass  $\sim m_W$  and is thus light enough to be on-shell produced at LEP, is to employ the type-I two Higgs doublet model (2HDM-I). In this model, all the  $H^\pm$ -fermion couplings are suppressed like  $1/\tan\beta$ , the ratio of the two vacuum expectation values (VEVs). With the choice of a high enough  $\tan\beta$ , this enables  $H^\pm$  to escape from the severe flavour changing neutral current (FCNC) constraints as well as any process that probes the  $H^\pm$ -fermion interaction such as  $Z \rightarrow b\bar{b}$ ,  $t \rightarrow bH^\pm$ , and  $B \rightarrow \tau\nu$ .

Presuming the above LEP anomaly to be real, the following points make this scenario more appealing. First, invoking a light charge Higgs (discussed also in [28]) is the only proposed solution that does not spoil the other precision lepton universality tests using lepton or meson decays [29]. Second, the requirement of a light charged Higgs plus  $b \rightarrow s\gamma$  singles out type-I out of the four types of 2HDMs [30] in which tree-level FCNC is forbidden by a  $Z_2$  symmetry [4]. Note that these assumptions already fix many aspects of the model that otherwise offer more than one option, i.e. the Yukawa coupling structure, the charged Higgs mass, and the viable range of  $\tan\beta$ . These combine to predict a distinct set of collider physics signatures.

In this paper, we shall consider  $CP$ -violation in the Higgs sector, which can in general occur in a class of 2HDMs. In this way, we can explore Higgs mixing patterns which received

relatively less attention. A practical advantage is that one can analyse both the scalar and the pseudo-scalar Higgses in a unified manner: switching between the two sectors reduces to tuning the Higgs mixing angles, which determine the composition of each neutral mass eigenstate.

Within the context of the Minimal Supersymmetric Standard Model (MSSM), there are earlier studies of  $CP$ -violating Higgs phenomenology. In particular, the general  $CP$ -violating potential and mass spectrum can be found in the paper of A. Pilaftsis and C. Wagner [31], where the importance of the scalar–pseudo-scalar transitions in Higgs phenomenology was emphasised. In the same article, the couplings of the charged Higgs boson to  $CP$ -violating Higgs bosons were also discussed.

This article is organised as follows. We begin by giving an overview of the model in the next section. Section III is a summary of our search strategy, which leads to the main phenomenological results presented in section IV. Section V is devoted to the diphoton signal of the lightest neutral Higgs. We deliver our conclusion in section VI. In addition, we present: the ghost Lagrangian for our setup of 2HDM in appendix A, the relation between our parametrisation and perturbativity in appendix B, and differential cross-sections of our main process in appendix C.

## II. SETUP

### A. Model

Let us give a brief description of the type-I 2HDM that we have chosen. The type of a 2HDM refers to one of the multiple ways to organise the Yukawa couplings. There are four types in which quarks or leptons of each charge couple to only one Higgs doublet [30], so that neutral Higgses are naturally prevented from mediating FCNC [32]. To this end, we impose the softly broken  $Z_2$  symmetry, under which the two Higgs doublets  $\Phi_{1,2}$  transform as

$$(\Phi_1, \Phi_2) \rightarrow (-\Phi_1, +\Phi_2), \quad (1)$$

whereas the fermion fields remain unchanged. This allows only the following Yukawa couplings,

$$-\mathcal{L}_Y = \bar{L}_L \Phi_2 Y_e e_R + \bar{Q}_L \Phi_2 Y_d d_R + \bar{Q}_L \epsilon \Phi_2^* Y_u u_R + \text{h.c.}, \quad (2)$$

between  $\Phi_2$  and fermions, so all the fermions acquire mass from the VEV of  $\Phi_2$  [10].

The scalar potential including the soft  $Z_2$ -breaking terms reads

$$\begin{aligned} V = & \frac{\lambda_1}{2}(\Phi_1^\dagger \Phi_1)^2 + \frac{\lambda_2}{2}(\Phi_2^\dagger \Phi_2)^2 + \lambda_3(\Phi_1^\dagger \Phi_1)(\Phi_2^\dagger \Phi_2) \\ & + \lambda_4(\Phi_1^\dagger \Phi_2)(\Phi_2^\dagger \Phi_1) + \frac{1}{2} \left[ \lambda_5(\Phi_1^\dagger \Phi_2)^2 + \text{h.c.} \right] \\ & - \frac{1}{2} \left\{ m_{11}^2(\Phi_1^\dagger \Phi_1) + \left[ m_{12}^2(\Phi_1^\dagger \Phi_2) + \text{h.c.} \right] + m_{22}^2(\Phi_2^\dagger \Phi_2) \right\}. \end{aligned} \quad (3)$$

In unitary gauge, the Higgs doublet fields are expanded around the minimum like

$$\Phi_1 = \begin{bmatrix} i \sin \beta H^+ \\ \frac{1}{\sqrt{2}}(v_1 + \eta_1 - i \sin \beta \eta_3) \end{bmatrix}, \quad \Phi_2 = \begin{bmatrix} -i \cos \beta H^+ \\ \frac{1}{\sqrt{2}}(v_2 + \eta_2 + i \cos \beta \eta_3) \end{bmatrix}. \quad (4)$$

One can take a basis of  $\Phi_{1,2}$  such that  $v_1$  and  $v_2$  are both real. Their quadrature sum is subject to the constraint,  $v_1^2 + v_2^2 = v^2$ , where  $v = 2^{-1/4} G_F^{-1/2}$  is the SM Higgs VEV. Their ratio is parametrised by

$$\tan\beta = v_2/v_1, \quad (5)$$

in terms of the pseudo-scalar and charged Higgs mixing angle  $\beta$ .

We introduce  $CP$ -violation in the Higgs sector by assuming  $\text{Im}\lambda_5 \neq 0$  and  $\text{Im}m_{12}^2 \neq 0$ , which enables the neutral scalar and pseudo-scalar components to mix together. The real symmetric mass-squared matrix  $\mathcal{M}^2$  with respect to the basis  $(\eta_1, \eta_2, \eta_3)$ , is diagonalised by the mass eigenstates

$$H_i = R_{ij}\eta_j, \quad i, j = 1, 2, 3, \quad (6)$$

like

$$R\mathcal{M}^2 R^T = \text{diag}(M_1^2, M_2^2, M_3^2), \quad (7)$$

using a  $3 \times 3$  orthogonal matrix  $R$ . It is parametrised in terms of the mixing angles  $\alpha_{1,2,3}$  in the form,

$$R = \begin{bmatrix} c_1 c_2 & s_1 c_2 & s_2 \\ -(c_1 s_2 s_3 + s_1 c_3) & c_1 c_3 - s_1 s_2 s_3 & c_2 s_3 \\ -c_1 s_2 c_3 + s_1 s_3 & -(c_1 s_3 + s_1 s_2 c_3) & c_2 c_3 \end{bmatrix}, \quad (8)$$

where  $s_i = \sin \alpha_i$  and  $c_i = \cos \alpha_i$ . The neutral Higgs mass eigenvalues are assumed to be in the order,

$$M_1^2 \leq M_2^2 \leq M_3^2. \quad (9)$$

This determines the following physical domain of the mixing angles [33]:

$$-\pi/2 < \alpha_{1,2,3} \leq \pi/2. \quad (10)$$

The two  $CP$ -violating mass matrix elements are related by [34]

$$(\mathcal{M}^2)_{13} = \tan\beta(\mathcal{M}^2)_{23}, \quad (11)$$

which translates into the constraint,

$$M_3^2 = \frac{M_1^2 R_{13}(R_{12} \tan\beta - R_{11}) + M_2^2 R_{23}(R_{22} \tan\beta - R_{21})}{R_{33}(R_{31} - R_{32} \tan\beta)}. \quad (12)$$

We shall remain in the parameter volume that is compatible with the mass ordering (9) in conjunction with (12), in order to avoid double counting of physically identical parameter sets.

Two more dimensionful quantities can be derived from the scalar potential: the charged Higgs mass,

$$M_{H^\pm}^2 = \mu^2 - \frac{1}{2}v^2(\lambda_4 + \text{Re}\lambda_5), \quad (13)$$

and the auxiliary parameter,

$$\mu^2 = \text{Re} m_{12}^2 / \sin 2\beta, \quad (14)$$

that sets the mass scale of charged/neutral Higgs particles except  $H_1$ .

We have the eight physical quantities determined from the Higgs potential,

$$M_1, M_2, M_{H^\pm}, \alpha_1, \alpha_2, \alpha_3, \mu, \tan\beta. \quad (15)$$

In this work, we opt to invert this dependency and express the parameters appearing in (3) in terms of those in (15) [34]. The mass parameters are then given by

$$m_{11}^2 = \lambda_1 v_1^2 + (\lambda_3 + \lambda_4 + \text{Re}\lambda_5 - 2\nu) v_2^2, \quad (16a)$$

$$m_{22}^2 = \lambda_2 v_2^2 + (\lambda_3 + \lambda_4 + \text{Re}\lambda_5 - 2\nu) v_1^2, \quad (16b)$$

$$\text{Im} m_{12}^2 = \text{Im}\lambda_5 v_1 v_2, \quad (16c)$$

with  $\nu = \mu^2/v^2$  and  $\text{Re} m_{12}^2$  fixed by (14). The quartic couplings are

$$\begin{aligned} \lambda_1 = & \frac{1}{c_\beta^2 v^2} [c_1^2 c_2^2 M_1^2 + (c_1 s_2 s_3 + s_1 c_3)^2 M_2^2 \\ & + (c_1 s_2 c_3 - s_1 s_3)^2 M_3^2 - s_\beta^2 \mu^2], \end{aligned} \quad (17a)$$

$$\begin{aligned} \lambda_2 = & \frac{1}{s_\beta^2 v^2} [s_1^2 c_2^2 M_1^2 + (c_1 c_3 - s_1 s_2 s_3)^2 M_2^2 \\ & + (c_1 s_3 + s_1 s_2 c_3)^2 M_3^2 - c_\beta^2 \mu^2], \end{aligned} \quad (17b)$$

$$\begin{aligned} \lambda_3 = & \frac{1}{c_\beta s_\beta v^2} \{c_1 s_1 [c_2^2 M_1^2 + (s_2^2 s_3^2 - c_3^2) M_2^2 \\ & + (s_2^2 c_3^2 - s_3^2) M_3^2] + s_2 c_3 s_3 (c_1^2 - s_1^2) (M_3^2 - M_2^2)\} \\ & + \frac{1}{v^2} (2M_{H^\pm}^2 - \mu^2), \end{aligned} \quad (17c)$$

$$\lambda_4 = \frac{1}{v^2} [s_2^2 M_1^2 + c_2^2 s_3^2 M_2^2 + c_2^2 c_3^2 M_3^2 + \mu^2 - 2M_{H^\pm}^2], \quad (17d)$$

$$\text{Re}\lambda_5 = \frac{1}{v^2} (-s_2^2 M_1^2 - c_2^2 s_3^2 M_2^2 - c_2^2 c_3^2 M_3^2 + \mu^2), \quad (17e)$$

$$\begin{aligned} \text{Im}\lambda_5 = & \frac{-1}{c_\beta s_\beta v^2} \{c_\beta [c_1 c_2 s_2 M_1^2 - c_2 s_3 (c_1 s_2 s_3 + s_1 c_3) M_2^2 \\ & + c_2 c_3 (s_1 s_3 - c_1 s_2 c_3) M_3^2] + s_\beta [s_1 c_2 s_2 M_1^2 \\ & + c_2 s_3 (c_1 c_3 - s_1 s_2 s_3) M_2^2 - c_2 c_3 (c_1 s_3 + s_1 s_2 c_3) M_3^2]\}, \end{aligned} \quad (17f)$$

where  $s_\beta = \sin\beta$ ,  $c_\beta = \cos\beta$ .

In this approach, the solutions for  $\lambda_{1,\dots,5}$  may turn out to be non-perturbatively large, unless one takes care to set the input parameters in (15) to sensible values. To avoid entering a nonsensical regime, we shall check that the sizes of the Higgs quartic couplings meet the conditions,

$$|\lambda_i| \leq 4\pi, \quad i = 1, \dots, 5. \quad (18)$$

Another theoretical constraint on the quartic couplings that is closely related to perturbativity arises from the tree-level unitarity in Higgs-Higgs scattering. We also take this into account using the formulation in [35]. As we find in the numerical analysis, this perturbative unitarity is always satisfied as long as we require (18), within the parameter space explored in this work.

The interactions of Higgs bosons with other particles are described by the Lagrangian,

$$\Delta\mathcal{L} = \sum_{i=1}^2 (D^\mu \Phi_i)^\dagger (D_\mu \Phi_i) + \mathcal{L}_Y, \quad (19)$$

$H_i \bar{u}_j u_j$	$-i(m_{u_j}/v)(R_{i2}/\sin\beta - iR_{i3}\cot\beta\gamma^5)$
$H_i \bar{d}_j d_j$	$-i(m_{d_j}/v)(R_{i2}/\sin\beta + iR_{i3}\cot\beta\gamma^5)$
$H^+ \bar{u}_j d_k$	$\sqrt{2}(\cot\beta/v)V_{jk}(m_{u_j}P_L - m_{d_k}P_R)$
$H_i \bar{l}_j l_j$	$-i(m_{l_j}/v)(R_{i2}/\sin\beta + iR_{i3}\cot\beta\gamma^5)$
$H^+ \bar{\nu}_j l_j$	$-\sqrt{2}(\cot\beta/v)m_{l_j}P_R$
$H_i W_\mu^+ W_\nu^-$	$i(2m_W^2/v)(R_{i1}\cos\beta + R_{i2}\sin\beta)g_{\mu\nu}$
$H_i Z_\mu Z_\nu$	$i(2m_Z^2/v)(R_{i1}\cos\beta + R_{i2}\sin\beta)g_{\mu\nu}$
$H_i H^+ W_\mu^-$	$i(m_W/v)[(R_{i1}\sin\beta - R_{i2}\cos\beta)i - R_{i3}](p + p')_\mu$

TABLE I. Feynman rules. The momentum directions are indicated in figure 2. The chirality projection matrices are defined by  $P_{L/R} = (1 \mp \gamma^5)/2$ .

with  $\mathcal{L}_Y$  from (2). One expands the covariant derivatives, replaces  $\Phi_{1,2}$  by (4), and diagonalises the fermion and Higgs mass terms, to arrive at the Feynman rules in table I. They will be used to calculate and interpret the results that we present in the following sections.

A remark is in order regarding the parametrisation in the  $CP$ -conserving limit. One can enforce  $CP$ -conservation simply by setting  $\alpha_2 = \alpha_3 = 0$ . This eliminates mixing between the  $CP$ -odd and the  $CP$ -even degrees-of-freedom, as can be seen in (8). The mixing between  $\eta_1$  and  $\eta_2$  with the angle  $\alpha = \alpha_1 - \pi/2$ , results in the lighter and the heavier  $CP$ -even neutral eigenstates,  $h$  and  $H$ . The  $CP$ -odd neutral Higgs  $A$  is identified with  $\eta_3$ . In this case, the relation (11) becomes trivial and therefore it no longer constrains  $M_3^2$  to be determined as a function of the other parameters. As a result, we are left with two less mixing angles and one more free mass parameter in the  $CP$ -conserving Higgs sector than in the  $CP$ -violating case. Conventionally, these seven free parameters are chosen to be:  $M_h, M_H, M_A, M_{H^\pm}, \alpha, \beta, \mu$  [36].

## B. Parameter space

Having established the framework, one should fix the range of parameters to study. For future references, we first collect the values which were chosen for the reasons explained below:

$$M_{H^\pm} = 86 \text{ GeV}, \quad M_1 = 125 \text{ GeV}, \quad M_2 = 200 \text{ GeV}, \quad \mu = 100 \text{ GeV}, \quad \tan\beta = 5. \quad (20)$$

This set shall be used by default throughout the analysis unless specified otherwise, in combination with one of the two Higgs mixing configurations,

$$(\sin\alpha_1, \sin\alpha_2, \sin\alpha_3) = \begin{cases} (-0.6, 0.1, 0.5), & \text{benchmark point } P_1, \\ (0.0, 0.8, 0.5), & \text{benchmark point } P_2. \end{cases} \quad (21)$$

The charged Higgs mass is more or less predetermined by the LEP data. The lower bound is provided by the direct search, and the upper limit comes from the requirement that the  $H^\pm$  pair production should restore lepton universality in leptonic  $W$  decays. We take  $M_{H^\pm}$  which reduces the apparent discrepancy between  $\mathcal{B}(W \rightarrow \tau\nu)$  and the average of

$\mathcal{B}(W \rightarrow e\nu)$  and  $\mathcal{B}(W \rightarrow \mu\nu)$  by  $1\sigma$  [21]. The latest update from the OPAL collaboration reports the direct search limit,  $M_{H^\pm} > 82$  GeV, for  $M_A \geq M_{H^\pm}$  at 95% confidence level (CL) [37]. In view of the recent evidences from ATLAS [25] and CMS [26], we set the lightest neutral Higgs mass to 125 GeV. The heavier Higgs mass parameter is taken to be fairly higher than  $M_1$ . Non-degenerate mass spectrum is needed for  $CP$ -violating Higgs mixing. The last dimensionful parameter  $\mu$  is set to a representative value of the weak scale order.

The chosen  $M_2$  is a mass at which the SM Higgs production is strongly constrained at the LHC. Not far from there lies also  $M_3 \lesssim 300$  GeV. In this range, the rates of the  $WW$  and  $ZZ$  channels are limited to be roughly below half their SM predictions [38]. In our model, the upper bounds must be reinterpreted as arising from processes mediated by  $H_2$  and  $H_3$  whose interactions are different from those of the SM Higgs. For this, we require that

$$\sigma(gg \rightarrow H_{2,3} \rightarrow WW/ZZ) < 0.5 \sigma(gg \rightarrow h_{\text{SM}} \rightarrow WW/ZZ). \quad (22)$$

A potentially important constraint is provided by the  $\rho$  parameter [39]. With the Higgs mass spectrum assumed in this work, one can check that the one-loop correction from the Higgs bosons to  $\rho$  is small enough to pass the electroweak precision tests [21, 40].

For safety of a light charged Higgs, it is crucial to choose a high enough  $\tan\beta$ . The strongest bound is given by  $b \rightarrow s\gamma$ , which requires  $\tan\beta \gtrsim 4$  [21]. This range of  $\tan\beta$  also suppresses  $\mathcal{B}(t \rightarrow bH^+)$  below 4%. This maximal top-quark branching fraction coincides roughly with the numerical values of the 95% CL limits from the light charged Higgs searches at the LHC [41]. However, these LHC constraints on  $t \rightarrow bH^+$  are based on the assumption that  $\mathcal{B}(H^\pm \rightarrow \tau\nu) = 1$ , and therefore become weaker in our setup where  $\mathcal{B}(H^\pm \rightarrow \tau\nu) = 0.7$ . In principle, one could use any  $\tan\beta$  larger than the FCNC bound, as long as it lets the charged Higgs decay inside the detector. In practice, it is bounded from above by perturbativity through (17). Obviously, this upper limit is a function of the other parameters. In appendix B, it is shown that  $\mu$  can always be adjusted so that perturbativity holds. One should not regard this as a fine-tuning but rather an artifact of the employed parametrisation. If one started by setting the parameters appearing in (3) and then derived the quantities in (15), then one could trivially satisfy perturbativity by keeping  $\lambda_{1,\dots,5}$  inside the range (18). Even in this reverse approach, one could naturally obtain a high  $\tan\beta$ , as one can see from the example of inert doublet model where an exact  $Z_2$  symmetry leads to infinite  $\tan\beta$  [13].

Among the three remaining Higgs mixing angles, we scan  $\alpha_1$  and  $\alpha_2$  which determine the composition of the lightest neutral Higgs. In (8), one can notice that  $\sin\alpha_2$  is the fraction of the  $CP$ -odd component in  $H_1$ . We fix  $\sin\alpha_3$  to 0.5 to have an intermediate level of  $CP$ -violation. For illustrative purposes, we select two benchmark points, labelled  $P_1$  and  $P_2$  in (21). The fraction of  $A$  in  $H_1$  is chosen to be small at  $P_1$  and large at  $P_2$ .

### III. LIGHT $H^\pm$ SEARCH STRATEGY

Given the model and the input parameters, we consider which charged Higgs production mechanism is most useful. We first calculate the cross-sections of the following standard



channels:

$$q\bar{q} \rightarrow W \rightarrow H_1 H^\pm, \quad (23a)$$

$$qq \rightarrow jj + H_i \rightarrow jj + WH^\pm, \quad (23b)$$

$$q\bar{q} \rightarrow W + H_i \rightarrow W + WH^\pm, \quad (23c)$$

$$q\bar{q} \rightarrow Z + H_i \rightarrow Z + WH^\pm, \quad (23d)$$

$$gg \rightarrow H_i \rightarrow WH^\pm, \quad (23e)$$

$$gb \rightarrow tH^-, \quad (23f)$$

$$gg, q\bar{q} \rightarrow t\bar{b} + H^+. \quad (23g)$$

The last two entries are meant to imply their conjugate processes as well. The final state in (23g) can be made through either top pair production or gluon-gluon fusion [42].

In figures 1, we plot the cross-sections against  $\tan\beta$  for the two benchmark points. One observes the general tendency that each production rate is depleted for high  $\tan\beta$ . As one can expect from table I, processes (23f) and (23g) die out as  $\tan\beta$  grows, while the others approach their individual asymptotic cross-sections even though many of them are small.

An outstanding exception is the production associated with a neutral Higgs (23a), which is not suppressed even for high  $\tan\beta$ . The diagrams for this process are shown in figure 2, which scale according to the  $H_i$ - $H^\pm$ - $W$  vertices in table I. In the  $H_1$ - $H^\pm$ - $W$  interaction, the pseudo-scalar coupling is proportional to  $\sin\alpha_2$  and independent of  $\beta$ , and the scalar coupling is proportional to  $\cos\alpha_1 \cos\alpha_2$  in the limit of  $\tan\beta \rightarrow \infty$ . Combining these two behaviours, one can expect that the  $H_1 H^\pm$  production becomes efficient unless  $|\sin\alpha_1|$  is large and  $|\sin\alpha_2|$  is small.

The results plotted in figures 1 do not depend on  $\mu$ . Therefore, they remain valid even if one adjusts  $\mu$  for the perturbativity of  $\lambda_{1,\dots,5}$  in the high  $\tan\beta$  regime. This means that the production mechanism (23a) is of the most general interest among the displayed channels, and we shall focus on it in what follows. Note that the same type of diagram was previously considered in the contexts of the MSSM [43] and a fermiophobic Higgs scenario [44].

The next step should be to select the decay products of  $H^\pm$  and  $H_1$ . The two dominant branching ratios of  $H^+$  are

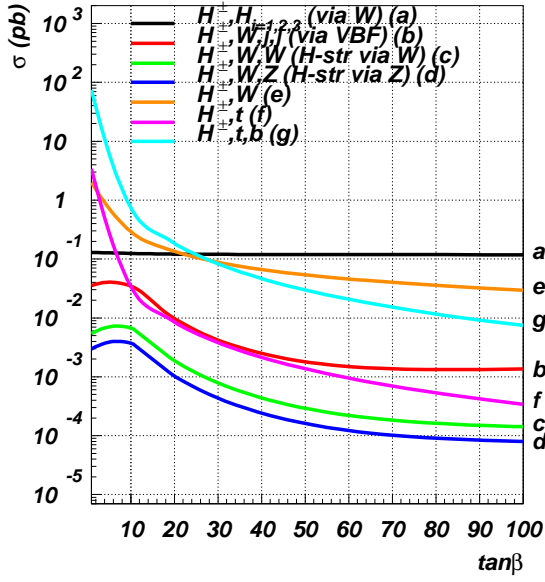
$$\mathcal{B}(H^+ \rightarrow \tau^+ \nu_\tau) = 0.71, \quad \mathcal{B}(H^+ \rightarrow c\bar{s}) = 0.27, \quad (24)$$

as long as  $M_{H^\pm} \lesssim 135$  GeV, beyond which the charged Higgs decays mediated by a virtual top becomes non-negligible [45]. These branching fractions are essentially independent of any of the input parameters. This is a notable feature of the 2HDMI, stemming from the universal scaling behaviour of the  $H^\pm$ -fermion couplings: they are all proportional to  $\cot\beta$ , as shown in table I. As we are mainly interested in a charged Higgs that is light enough to have been produced at LEP energies, we can regard (24) as good approximations and simply choose the decay product with the highest rate,  $\tau\nu$ .

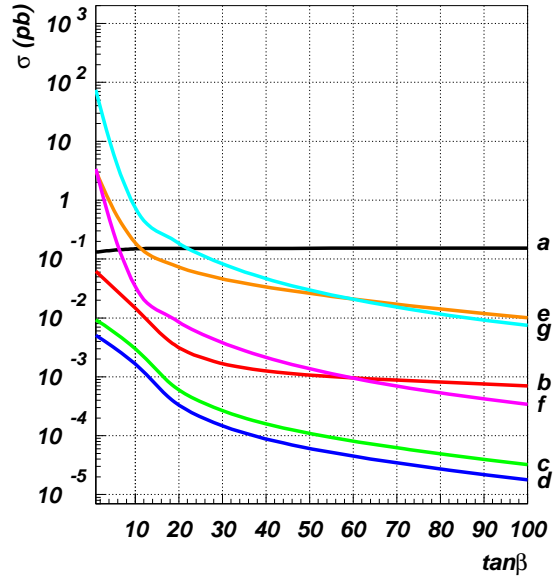
As for  $H_1$ , we plot its branching fractions in the vicinity of  $M_1 = 125$  GeV, in figures 3. One finds that the  $b\bar{b}$  mode is dominant at both benchmark points. This tends to be the case unless both  $\sin\alpha_1$  and  $\sin\alpha_2$  are vanishingly small. At the point where  $\sin\alpha_1 = \sin\alpha_2 = 0$ , the tree-level  $H_1$ -fermion coupling vanishes, causing its fermiophobia. Considering these dominant decay modes of  $H^\pm$  and  $H_1$ , we are going to concentrate on the final state,  $\tau\nu b\bar{b}$  for numerical simulation.

One can also notice that the branching fractions of the  $\gamma\gamma$  and  $gg$  modes can differ significantly from their individual SM values. Albeit not directly related to the charged

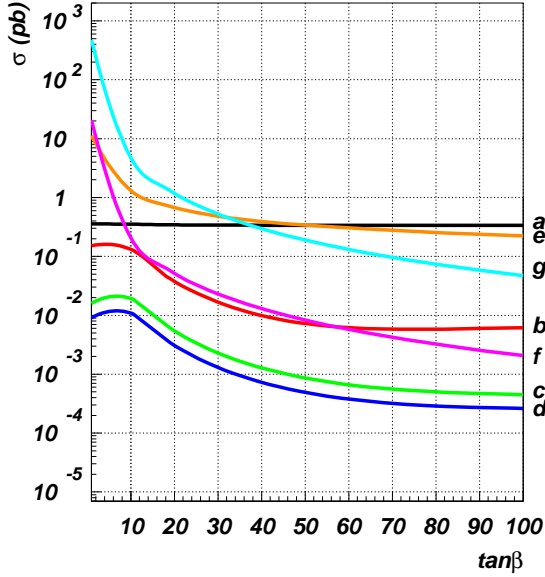




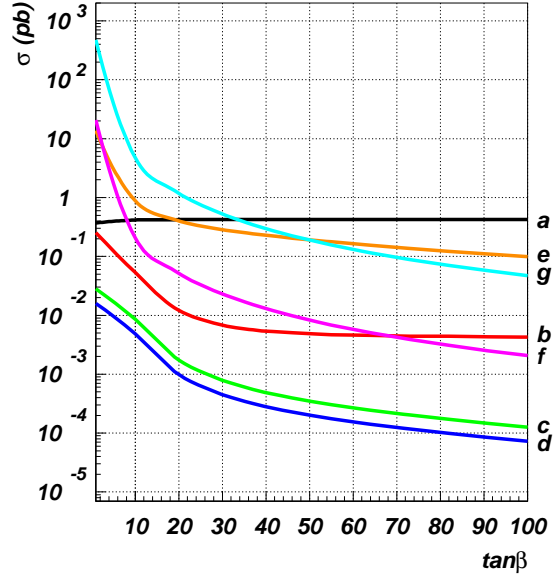
(a)  $P_1$ ,  $\sqrt{s} = 7$  TeV



(b)  $P_2$ ,  $\sqrt{s} = 7$  TeV



(c)  $P_1$ ,  $\sqrt{s} = 14$  TeV



(d)  $P_2$ ,  $\sqrt{s} = 14$  TeV

FIG. 1. Cross-sections of the single charged Higgs production mechanisms plotted against  $\tan\beta$  for the selected benchmark points and centre-of-mass energies. The curves are independent of  $\mu$ .

Higgs search, these changes greatly affect the phenomenology of  $H_1$ . We shall come back to this issue in section V.

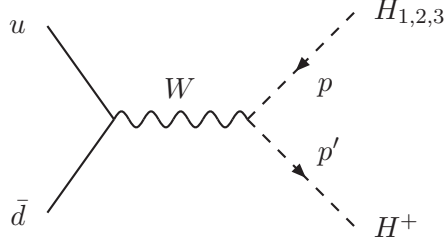


FIG. 2. Feynman graph for the charged Higgs production in association with a neutral Higgs.

#### IV. LHC PROSPECTS OF $H^\pm$ SEARCH

The main process of our concern is  $pp \rightarrow W \rightarrow H^\pm H_1$ , followed by the decays,  $H^\pm \rightarrow \tau \nu$  and  $H_1 \rightarrow b\bar{b}$  at the LHC. Among these three subprocesses, the charged Higgs production and decay revealed their outstanding stability under variation of  $\tan\beta$  over a wide range, in the preceding section.

We shall envisage two experimental conditions at the LHC, which we call the “early” and the “full” searches. The “early search” denotes the centre-of-mass energy of the current run,  $\sqrt{s} = 7$  TeV, and the integrated luminosity of  $L = 10 \text{ fb}^{-1}$ . We assume that the “full search” will deliver  $L = 100 \text{ fb}^{-1}$  at  $\sqrt{s} = 14$  TeV.

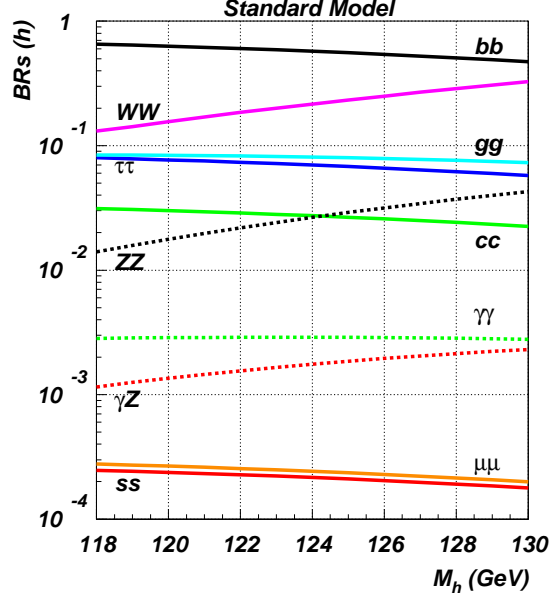
The kinematics of the  $\tau \nu b\bar{b}$  state can be fully reconstructed with high efficiency as it has only one neutrino. We assume a  $\tau$ -reconstruction efficiency  $\sim 100\%$  and a  $b$ -tagging efficiency  $\sim 70\%$ , plus the following set of selection cuts:

$$\begin{aligned}
 p_T(\bar{b}^{(-)}), p_T(\tau^\pm) &> 25 \text{ GeV}, \\
 |\eta(\bar{b}^{(-)})|, |\eta(\tau^\pm)| &< 2.5, \\
 p_T(\bar{\nu}^{(-)}) &> 20 \text{ GeV}, \\
 |\eta(\bar{\nu}^{(-)})| &< 4.5, \\
 M(b, \bar{b}) &= M_1 \pm 10 \text{ GeV},
 \end{aligned} \tag{25}$$

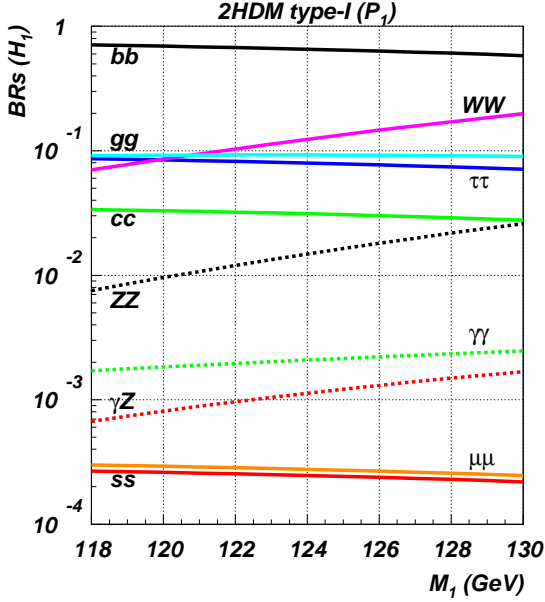
which we choose considering the operation of ATLAS. Assuming these cuts, we calculated the SM background.<sup>1</sup> The cross-section is  $\sigma(pp \rightarrow \tau^\pm \nu b\bar{b})_{\text{BG}} \simeq 55 \text{ fb}$  at  $\sqrt{s} = 7$  TeV and  $\simeq 110 \text{ fb}$  at  $\sqrt{s} = 14$  TeV.

Along with the associated production of  $H^\pm H_1$ , we also study a similar process with  $H^\pm$  replaced by  $W$ , i.e.  $pp \rightarrow W \rightarrow WH_1$ . As we shall see, the parameter space covered by this Higgs-strahlung is complementary to the region accessible to the  $H^\pm H_1$  state. We select the final state,  $l^\pm \nu b\bar{b}$  with  $l = e, \mu$ , and assume a  $W$ -reconstruction efficiency  $\sim 100\%$ . The cuts in (25) are used again, and the same cut on  $\tau$  is applied on the transverse momenta of the light leptons,  $p_T(l^\pm) > 25 \text{ GeV}$ . Using these parameters, we obtain the Higgs-less SM background cross-section to be  $\sigma(pp \rightarrow l^\pm \nu b\bar{b})_{\text{BG}} \simeq 70 \text{ fb}$  at  $\sqrt{s} = 7$  TeV and  $\simeq 140 \text{ fb}$  at  $\sqrt{s} = 14$  TeV.

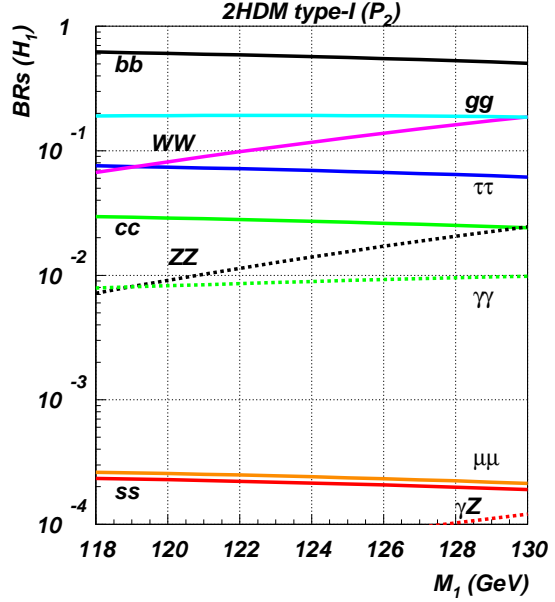
<sup>1</sup> Including contributions from a SM Higgs with mass of 125 GeV.



(a) SM



(b) 2HDM I,  $P_1$



(c) 2HDM I,  $P_2$

FIG. 3. Branching ratios of the (lightest) neutral Higgs plotted against its mass. The SM case is shown in panel 3a. Panels 3b and 3c are respectively for the benchmark points  $P_1$  and  $P_2$  in the 2HDM I. The parameters are set as in (20) unless stated otherwise.

We used LanHEP [46] to implement the model, and CalcHEP [47] plus the CTEQ6M parton distribution functions [48], to perform the phenomenological analysis. The Passarino-Veltman functions appearing in the effective vertices of  $H_i$ - $g$ - $g$  and  $H_i$ - $\gamma$ - $\gamma$  are calculated by calling the LoopTools package [49].

We first check the rates of our main processes with  $\sin \alpha_2 = \sin \alpha_3 = 0$ . In this  $CP$ -

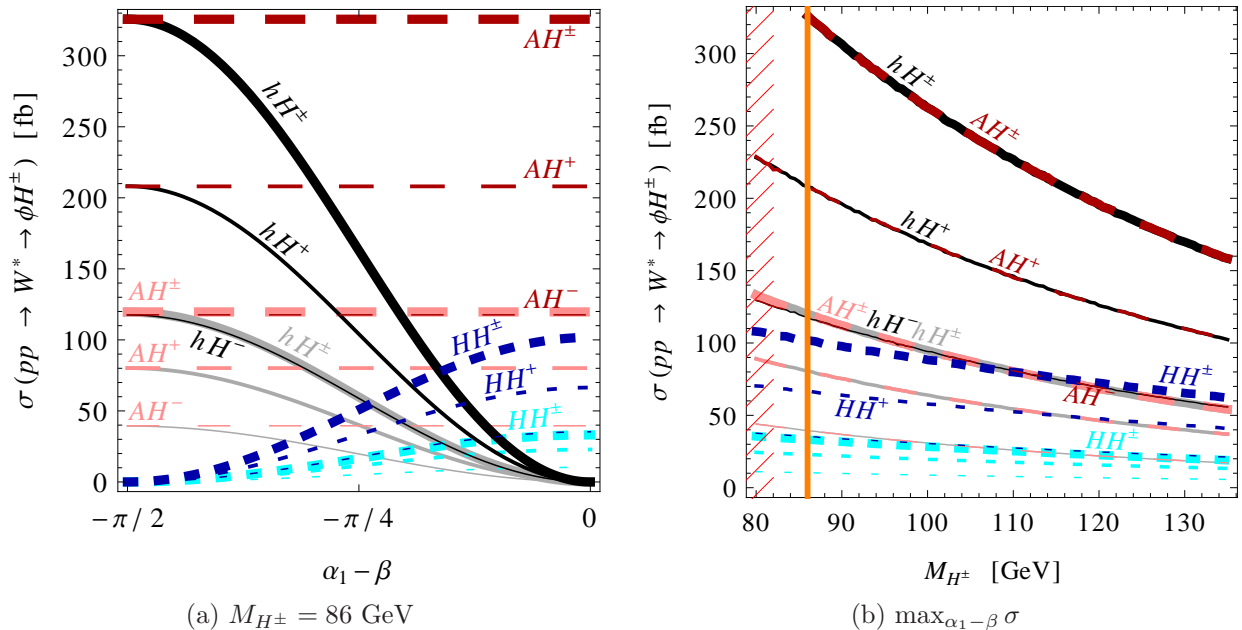
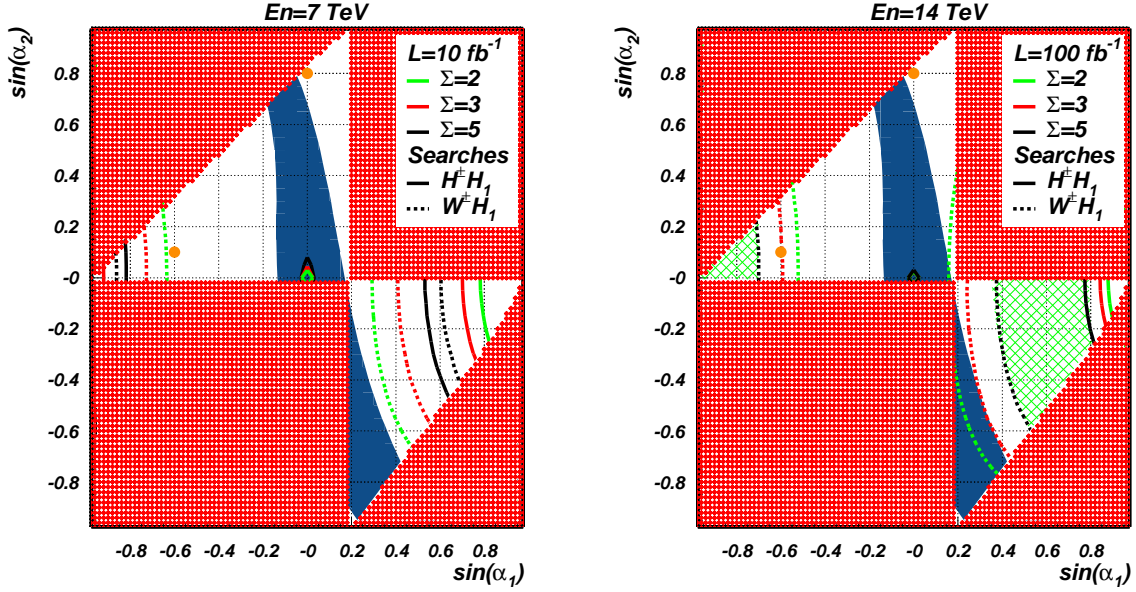


FIG. 4. Production cross-section of each neutral Higgs in association with a charged Higgs via a virtual  $W$ -boson in the  $CP$ -conserving case. The masses are  $M_h = M_A = 125$  GeV,  $M_H = 200$  GeV. For each channel, the lighter and the darker curves represent  $\sqrt{s} = 7$  TeV, 14 TeV, respectively. In panel 4b, the hatched region is excluded by LEP at 95% CL [37], and each curve is for  $\alpha_1 - \beta$  that maximises the cross-section.

conserving case, one has the lighter and the heavier  $CP$ -even Higgses,  $h \equiv H_1$  and  $H \equiv H_2$ , and the  $CP$ -odd Higgs,  $A \equiv H_3$ . The production cross-sections of  $h$ ,  $H$ , and  $A$ , each in association with a charged Higgs, are shown in figure 4a as functions of  $\alpha_1 - \beta$ . For each type of neutral Higgs, there are three curves that respectively represent  $H^-$ ,  $H^+$ , and  $H^\pm$  productions in the order of increasing thickness. The higher  $H^+$  rate relative to  $H^-$  reflects the fact that the LHC is a  $pp$  collider, not  $p\bar{p}$ . The shape of each curve is essentially determined by the dependence of the corresponding  $W$ - $H^\pm$ - $H_i$  coupling on  $\alpha_1$  and  $\beta$ , presented in table I. These patterns will be useful for understanding the simulation results to follow. From the plot, one can expect  $\mathcal{O}(10^4)$  events that occur through a charged-neutral Higgs associated production with the “full luminosity” at 14 TeV, unless the mixing angle is such that the given channel is highly suppressed.

Our analysis is of relevance to a light charged Higgs, even if one is not interested in a scenario where charged Higgs bosons have been on-shell produced at LEP energies. In this regard, it is legitimate to consider changes that would be caused by varying  $M_{H^\pm}$ . Obviously, the above production rates will be reduced as  $M_{H^\pm}$  grows, as is shown in figure 4b. We take the range of  $M_{H^\pm}$  up to  $\sim 135$  GeV, beyond which the charged Higgs decay pattern undergoes a qualitative change [45], thereby invalidating our assumptions given in (24). For  $M_{H^\pm} \sim 135$  GeV, each cross-section decreases roughly down to half the value in panel 4a. These curves illustrate the phase-space suppression that takes place for higher  $M_{H^\pm}$ . We emphasise that this reduction of statistics is the only essential information that one needs to understand how the significances would change in the following quantitative analysis with  $M_{H^\pm} = 86$  GeV, if one took a different  $M_{H^\pm}$ .



(a)  $\sqrt{s} = 7 \text{ TeV}, L = 10 \text{ fb}^{-1}$

(b)  $\sqrt{s} = 14 \text{ TeV}, L = 100 \text{ fb}^{-1}$

FIG. 5. Significance contours for the processes,  $pp \rightarrow H^\pm H_1 \rightarrow \tau^\pm \nu b \bar{b}$  (solid lines) and  $pp \rightarrow W^\pm H_1 \rightarrow l^\pm \nu b \bar{b}$  (dashed lines), on the  $(\sin \alpha_1, \sin \alpha_2)$  plane in the  $CP$ -violating case. The parameters are set as in (20) unless stated otherwise. Light grey (green online), dark grey (red online), and black correspond to the significances  $\Sigma = 2, 3, 5$ , respectively. The medium-shadowed regions (red online) are excluded by theoretical constraints. The dark-shadowed region (blue online) is ruled out by current limits on  $H_{2,3}$ . The light-shadowed region (green online) allows for discovery of both processes.

For the simulation of charged Higgs search, we turn on  $CP$ -violation allowing for mixing among all the three neutral Higgses,  $h$ ,  $H$ , and  $A$ . In figures 5, the contours of the significance  $\Sigma$  are shown for each process, which have been evaluated by means of the method described in [50]. There are two complications in comparison to the  $CP$ -conserving limit. One is that the additional mixing between the  $CP$ -odd and the  $CP$ -even components affects the significance of each process. The other is that  $M_{1,2,3}^2$  are no longer independent of one another but constrained by (12). In combination with the latter relation, the mass ordering (9) excludes the upper-right and the lower-left rectangular regions from the parameter domain. Another theoretical constraint that rules out the upper-left and the lower-right triangular regions, is perturbativity (18). We have also checked numerically that imposing perturbativity guarantees the tree-level unitarity in Higgs-Higgs scattering in the parameter space under consideration.

In addition to the above theoretical requirements, we impose the experimental constraints in (22) in order to respect the current Higgs production limits from the LHC. This rules out the dark-shadowed strip on the plane. The bounds on  $H_2$  and  $H_3$  apply as long as their masses are in the range between 160 and 600 GeV. All these conditions being fulfilled, the question to ask is how much portion of the remaining unshaded region the LHC can cover.

As in the preceding plot, the  $W$ - $H^\pm$ - $H_1$  coupling largely determines the shape of the  $H^\pm H_1$  contours. As long as one moves along the horizontal axis,  $H_1$  is purely  $CP$ -even,

and therefore its interactions not involving other neutral Higgses reduce to those of  $h$  in the  $CP$ -conserving Higgs sector.<sup>2</sup> For instance, the  $W$ - $H^\pm$ - $H_1$  coupling vanishes at the point  $(\sin \alpha_1, \sin \alpha_2) = (\sin \beta, 0) = (0.98, 0)$ , as is the case in figure 4a. This explains why the significance decreases as one approaches this point.

It should be meaningful to interpret the interesting behaviour of  $\Sigma$  around the point  $\alpha_1 = \alpha_2 = 0$ , although it belongs to the  $H_{2,3}$  exclusion strip. For instance, there might be a way to circumvent the constraint (22) by taking a different set of parameters. In the neighbourhood of this point, one finds a sudden drop of significance even though the  $W$ - $H^\pm$ - $H_1$  coupling stays nearly maximal. This is because the  $H_1$ - $b$ - $\bar{b}$  coupling is suppressed there as can be seen in table I. At the origin,  $H_1$  becomes fermiophobic, and its dominant decay modes are  $WW^*$  and  $ZZ^*$ . The fermiophobia of  $H_1$  generically gives rise to an enhanced  $\mathcal{B}(H_1 \rightarrow \gamma\gamma) \sim 1\%$  without the charged Higgs loop contribution. Including the  $H^\pm$ -loop, the diphoton branching fraction can range from zero up to  $\mathcal{O}(10\%)$ . [We give a related discussion in section V.] Therefore, the possibility of observing the  $H^\pm H_1$  state in the central low-significance hole via an alternative decay channel of  $H_1$  such as the  $\gamma\gamma$  mode, is highly dependent on the other model parameters.

As one departs away from the horizontal axis,  $\sin \alpha_2 = 0$ ,  $H_1$  acquires more of the  $CP$ -odd component. This reinforces the production rate of  $H^\pm H_1$  and thereby the significance, since the  $W$ - $H^\pm$ - $A$  coupling is not suppressed for any  $\alpha_1$  as can be seen in figure 4a.

Overall, figures 5 demonstrate that there is an ample portion of the parameter space in which the LHC has a good chance to discover the  $H^\pm H_1$  production. Obviously, the chance is substantially better in the “full luminosity” case, shown in figure 5b. With the exception of the narrow corners around both ends of the horizontal axis and the hole encircling the fermiophobic point, the discovery of  $H^\pm H_1$  through the  $\tau\nu b\bar{b}$  final state should be possible at any point in the unshaded physically sensible domain defined by (9), (18), and (22).

In the same figures is presented the  $H_1$ -strahlung process, which could also be detected depending on the mixing angles and the LHC operation condition. One can understand the shape of the  $W^\pm H_1$  contours by looking at the  $H_1$ - $W^+$ - $W^-$  coupling in table I. In figure 5a for “early searches”, one finds no common portion of the parameter space with  $\Sigma > 5$  for both processes. This setup predicts that it is not possible to discover both channels during the first data taking period in the  $l\nu b\bar{b}$  final states. Should this occur, this scenario will have to be modified to survive. In figure 5b, one finds a much broader region in which  $H_1$ -strahlung could be discovered. Part of this region is shadowed in light grey where the “full LHC” could observe both this process and  $H^\pm H_1$  production.

## V. IMPACT OF $H^\pm$ -LOOP ON $H_1 \rightarrow \gamma\gamma$

This section is devoted to phenomenology of the lightest neutral Higgs. In particular, we show that the charged Higgs loop can exert a marked influence on the  $H_1 \rightarrow \gamma\gamma$  decay mode, which is of the utmost importance in the neutral Higgs search at the LHC. We shall

---

<sup>2</sup> Nevertheless, the interactions of  $H_2$  and  $H_3$  do not reduce to those of  $H$  and  $A$  due to non-vanishing  $\sin \alpha_3$ .

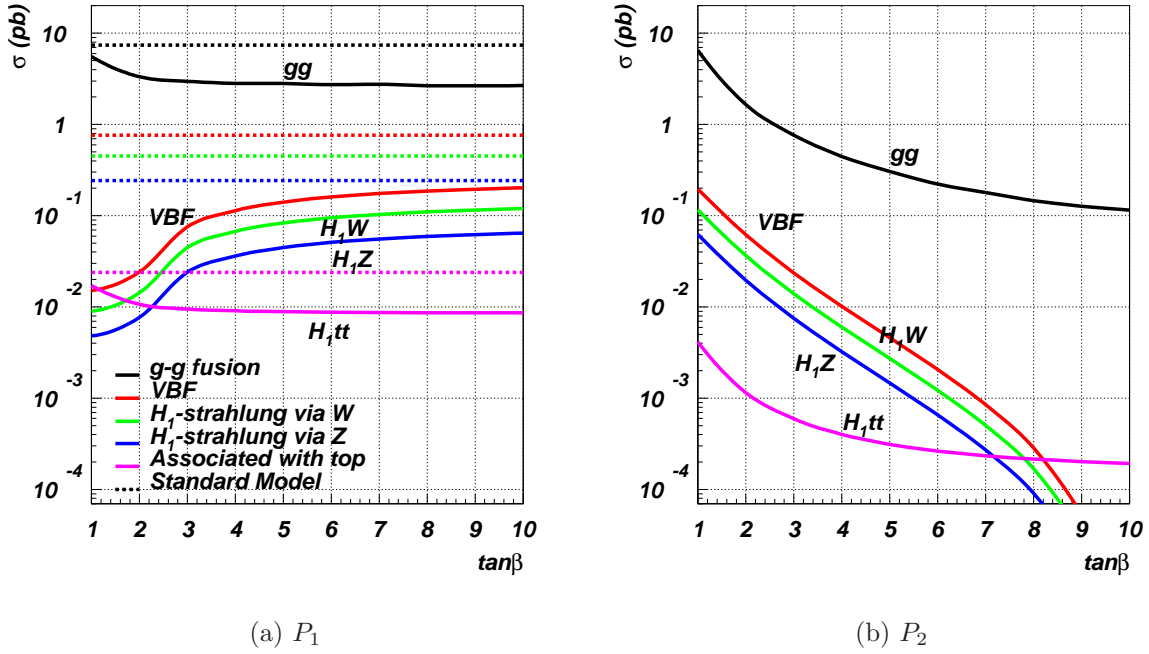


FIG. 6. Cross-sections of the lightest neutral Higgs production mechanisms plotted against  $\tan\beta$  at  $\sqrt{s} = 7$  TeV for the benchmark points  $P_1$  and  $P_2$ . The parameters are set as in (20) unless stated otherwise. The curves are independent of  $\mu$ .

consider the following standard Higgs production mechanisms:

$$\begin{aligned}
 gg &\rightarrow H_1 && (\text{gluon-gluon fusion}), \\
 qq &\rightarrow jj + H_1 && (\text{vector boson fusion}), \\
 q\bar{q} &\rightarrow W/Z + H_1 && (\text{Higgs-strahlung from } W/Z), \\
 gg, q\bar{q} &\rightarrow t\bar{t} + H_1 && (\text{associated production with a top-quark pair}).
 \end{aligned}$$

In figures 6, we plot the cross-sections of these channels at  $\sqrt{s} = 7$  TeV against  $\tan\beta$  for each of the two benchmark points. We have explicitly verified that all these production mechanisms are mostly unaffected in the range of  $M_1$  between 118 and 130 GeV and in the neighbourhood of the chosen  $M_{H^\pm}$ . All the production rates are lower than those in the SM. This is because of the suppression of the couplings in table I. Combining production and decay, we obtain an intriguing result:  $H_1$  may have escaped from the past and present searches due to the suppression of both its production and the branching ratios to massive vector boson pairs. As this scenario generically predicts lower rates into fermion pairs, it could be disfavoured by the recent hint in the  $b\bar{b}$  mode from the Tevatron [51] if it persists. Obviously, one can ease the reduction of  $H_1$  production by taking the Higgs mixing pattern to the SM-like limit,  $(\sin\alpha_1, \sin\alpha_2) = (1, 0)$ . In this case, the charged-neutral Higgs associated production will be suppressed as shown in figures 5. Recall that we are assuming a hierarchical neutral Higgs mass spectrum and that all the experimental evidences from the LHC and the Tevatron are caused by the lightest of the three neutral Higgs particles, which is also supposed to be produced in association with  $H^\pm$ . Relaxing one or more of these hypotheses may lead to a different consequence, although we do not explore this possibility in this paper.



On the other hand, branching fractions of the two loop-induced decay modes,  $H_1 \rightarrow \gamma\gamma$  and  $H_1 \rightarrow gg$ , have possibilities of being enhanced as well as diminished, depending on the input parameters. If they are increased, the suppressed Higgs production can be alleviated.

The decay into the digluon final state arises from the fermion loop, dominated by the top-quark contribution. Although the same type of loop is present also in the SM, its value can be different due to the variation of the  $H_1$ - $t$ - $\bar{t}$  coupling which is determined by the Higgs mixing angles as in table I. In particular, an interesting role is played by the  $CP$ -odd component  $A$  in  $H_1$  that could enhance the digluon branching fraction. Its effects are twofold: (a)  $A$  does not couple to a vector boson pair unlike the  $CP$ -even Higgs  $h$ ; (b) the digluon to difermion partial width ratio of  $A$  is higher than the corresponding quantity of  $h$ , i.e.

$$\frac{\Gamma(A \rightarrow gg)}{\Gamma(A \rightarrow f\bar{f})} = 2.3 \frac{\Gamma(h \rightarrow gg)}{\Gamma(h \rightarrow f\bar{f})}, \quad (26)$$

when  $M_A = M_h = 125$  GeV. This effect stems from the different Lorentz structures of the scalar and the pseudo-scalar couplings with fermions. The potential enhancement of the  $gg$  decay mode might be of interest at a future lepton collider experiment.

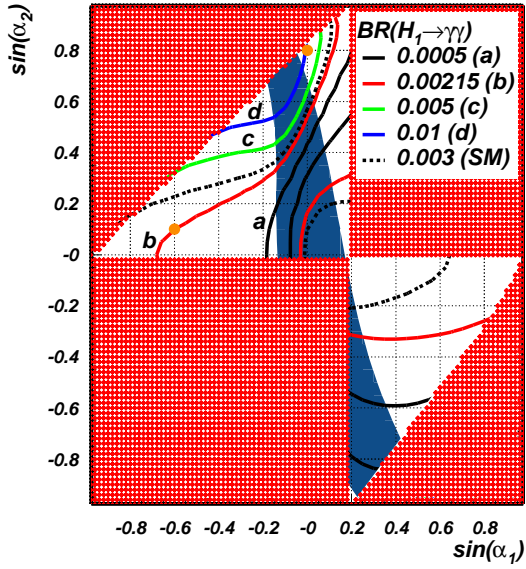
The decay amplitude of  $H_1 \rightarrow \gamma\gamma$  has two more components, the  $W$ - and the  $H^\pm$ -loops, in addition to the fermion loop. In the SM, the dominant contribution comes from the  $W$ -loop. Like the fermion loop, the  $W$ -loop can vary as a function of  $R_{ij}$ .

One might attempt to increase the diphoton branching fraction by invoking the same mechanism as with the digluon mode. As  $H_1$  becomes pseudo-scalar-like, the fermion loop alone does receive the relative enhancement that is given by (26) with  $gg$  replaced by  $\gamma\gamma$  and each numerator including only the fermion loop. However, this kills the  $W$ -loop at the same time, which is the dominant contribution in the SM. Therefore, a high  $CP$ -odd fraction in  $H_1$  is not really helpful in increasing  $\mathcal{B}(H_1 \rightarrow \gamma\gamma)$ .

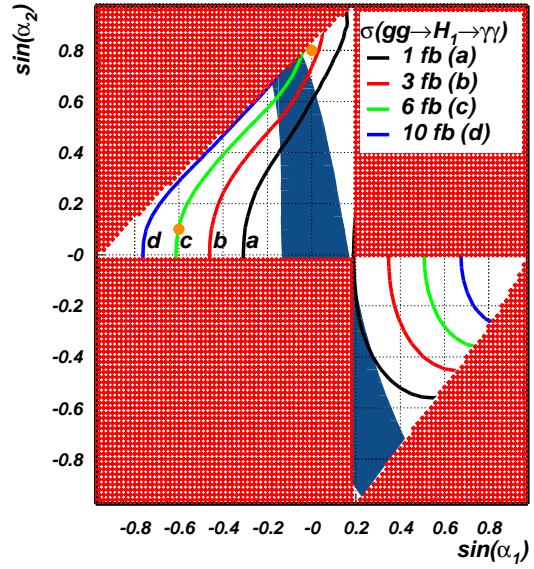
Nevertheless, it is known that the charged Higgs loop can greatly affect the  $\gamma\gamma$  mode when  $M_{H^\pm}$  is low [52–54]. In particular, this mechanism can lead to a high enough diphoton rate to be consistent with the excess surrounding the Higgs mass of 125 GeV recently observed by ATLAS [23] and CMS [24]. The  $H_1$ - $H^+$ - $H^-$  coupling depends on more parameters than the other loops, in particular on  $\mu$ , with which one can play in order to engineer the amplitude. The maximal permitted size of the  $H^\pm$ -contribution is mostly controlled by perturbativity and unitarity. In passing, we remark that change of  $\mu$  affects also  $\Gamma(H_{2,3} \rightarrow H^+H^-)$  and therefore the region excluded by (22), as we will see in the following plots.

To further study this potential variation, we plot the branching fraction of  $H_1 \rightarrow \gamma\gamma$  in figures 7a and 7c. Indeed, it can deviate substantially from its SM value depending on the mixing angles. One finds a valley between the two curves labelled “a” on each of the two plots, along which the branching ratio is highly suppressed. Across this valley, the  $H_1 \rightarrow \gamma\gamma$  amplitude flips its sign. As the plots show, the contours are deformed if  $\mu$  is changed, since they depend on the  $H^\pm$ -loop. One can also notice that part of the “d” contour of a high branching fraction lies on the verge of the perturbativity border, demonstrating that a sizeable  $H^\pm$ -loop contribution involves large quartic Higgs couplings.

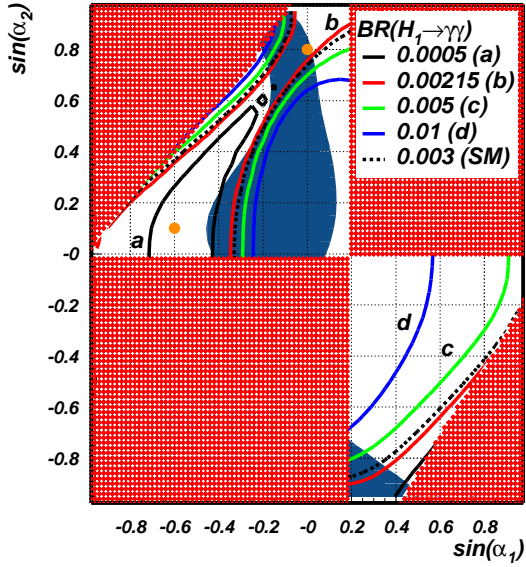
In conjunction with gluon-gluon fusion, this brings us to the cross-section of  $gg \rightarrow H_1 \rightarrow \gamma\gamma$  in figures 7b and 7d. With our crude leading-order approximation, it is estimated to be about 20 fb in the SM. In the entire region of panel 7b, the cross-section is smaller than its SM value due to the suppressed  $H_1$  production. Nevertheless, one still has the option to change  $\mu$  that affects the charged Higgs loop. For instance, the cross-section at  $(\sin \alpha_1, \sin \alpha_2) = (0.5, 0)$  is approximately 6 fb for  $\mu = 100$  GeV. At this point, the  $W$ -



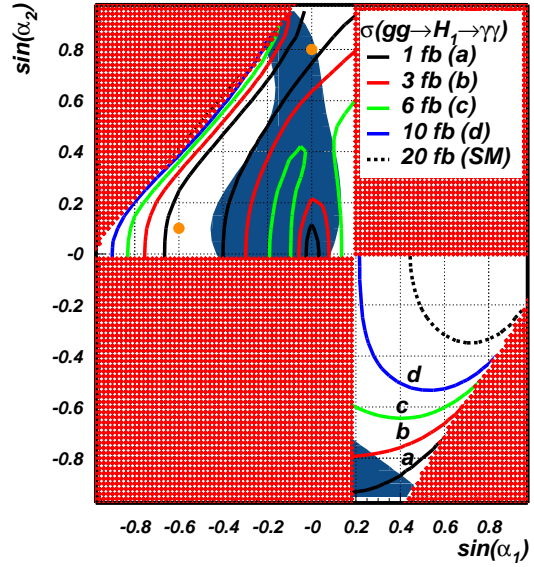
(a) Branching ratio,  $\mu = 100$  GeV



(b) Cross-section,  $\mu = 100$  GeV



(c) Branching ratio,  $\mu = 180$  GeV



(d) Cross-section,  $\mu = 180$  GeV

FIG. 7. Contours of the branching ratios and the cross-sections involving the diphoton final state on the  $(\sin \alpha_1, \sin \alpha_2)$  plane at  $\sqrt{s} = 7$  TeV. The two benchmark points  $P_1$  and  $P_2$  are marked by dots. The parameters are set as in (20) unless stated otherwise. The medium-shadowed regions (red online) are excluded by theoretical constraints. The dark-shadowed region (blue online) is ruled out by current limits on  $H_{2,3}$ .

and the  $H^\pm$ -loops interfere destructively. Taking  $\mu = 180$  GeV instead, one can make the interference constructive by flipping the sign of the  $H^\pm$ -contribution. This pushes the cross-section up above the SM prediction, as displayed in figure 7d. In this plot, the rate of  $gg \rightarrow H_1 \rightarrow \gamma\gamma$  can be comparable to its SM value even when the mixing angles are fairly removed from the SM-like point,  $(\sin \alpha_1, \sin \alpha_2) = (1, 0)$ . In combination with figures 5, this exhibits the exciting possibility that the LHC can discover a light charged Higgs in the foreseeable future while the recent evidences for Higgs decays to  $\gamma\gamma$  are partly due to the charged Higgs loop effect.

As one can expect, the charged Higgs loop effect weakens for high  $M_{H^\pm}$ . For instance,  $\mathcal{B}(H_1 \rightarrow \gamma\gamma)$  for  $M_{H^\pm} \sim 135$  GeV is roughly half its value for  $M_{H^\pm} = 86$  GeV, when one keeps  $(\sin \alpha_1, \sin \alpha_2) = (0.5, 0)$  and  $\mu = 180$  GeV.

## VI. CONCLUSIONS

We demonstrated the superb potential of the LHC to discover a light charged Higgs close to the  $W$ -boson mass in the  $CP$ -violating 2HDM1. For this purpose, we exploited the property of the  $pp \rightarrow W \rightarrow H_1 H^\pm$  process that its cross-section is stable against variation of  $\tan\beta$ , which can be anywhere above the lower bound placed by the most stringent FCNC constraints. We set the Higgs masses to their favoured values,  $M_{H^\pm} \sim 86$  GeV and  $M_1 \sim 125$  GeV, and found that the LHC can spot an excess in the  $\tau\nu b\bar{b}$  events, except in small corners and holes of the parameter space. We also examined the  $H_1$ -strahlung channel from  $W$ , which offers access to the complementary parameter volume to that of  $H_1 H^\pm$ .

With regard to  $CP$ -violation, we observed interesting consequences of the scalar–pseudo-scalar mixing. In particular,  $\mathcal{B}(H_1 \rightarrow gg)$  can be considerably affected by the composition of  $H_1$ . This result might be relevant to Higgs scrutiny at prospective linear collider experiments.

Motivated by the recent evidences for Higgs production at the LHC, we studied  $\sigma(gg \rightarrow H_1 \rightarrow \gamma\gamma)$ . Due to the Higgs mixing matrix elements appearing at interaction vertices, the production of  $H_1$  is generically suppressed in comparison to the SM. Nonetheless, the  $H^\pm$ -loop amplitude can make a constructive interference with the standard  $W$ -loop to raise  $\mathcal{B}(H_1 \rightarrow \gamma\gamma)$ . Depending on the parameter choice, this effect can be significant enough to increase the diphoton production rate from gluon-gluon fusion up to or even above the SM prediction. Alternatively, one can opt to enhance the  $H_1$  production itself by letting the Higgs mixing pattern approach the SM-like limit. In this case, the other processes with  $H_1$  going into the fermion and the massive vector boson pairs are also restored, the price to pay being suppression of the  $H_1 H^\pm$  rate.

Related to this last point, it may be beneficial to study further possibilities of the light charged Higgs scenario in which one makes assumptions different from those underlying the present article.

## ACKNOWLEDGMENTS

GMP would like to thank Per Osland and Alexander Pukhov for helpful discussions. JP thanks Eung Jin Chun for valuable comments and Kazuki Sakurai for the help with access to the literature. We acknowledge financial support from German Research Foundation DFG through Grant No. STO876/2–1 and BMBF.

## Appendix A: Gauge-fixing Lagrangian of the 2HDM

Assuming the 't Hooft-Feynman gauge, we choose a basis for the  $\Phi_i$  by expanding the Higgs doublets as

$$\Phi_1 = \begin{pmatrix} -i(c_\beta w^+ - s_\beta H^+) \\ \frac{v_1 + \eta_1 + i(c_\beta z - s_\beta \eta_3)}{\sqrt{2}} \end{pmatrix}, \quad \Phi_2 = \begin{pmatrix} -i(s_\beta w^+ + c_\beta H^+) \\ \frac{v_2 + \eta_2 + i(s_\beta z + c_\beta \eta_3)}{\sqrt{2}} \end{pmatrix}, \quad (\text{A1})$$

where  $w^\pm(z)$  is the Goldstone boson of  $W^\pm(Z)$ . We remark that the  $\eta_3$  pseudo-scalar field is orthogonal to the neutral Goldstone boson  $z$ .

As for the Goldstone boson mass spectrum, it is possible to find a convenient way to write the mass matrix. Having each  $\Phi_{1,2}$  the same group representation of the SM Higgs, following the notation of [55], in the gauge-Goldstone<sup>3</sup> basis we find the following representation of the co-variant derivative:

$$\mathcal{D}_{1,2} = \frac{v_{1,2}}{2} \begin{pmatrix} g & 0 & 0 \\ 0 & g & 0 \\ 0 & 0 & g \\ 0 & 0 & -g_1 \end{pmatrix}. \quad (\text{A2})$$

While the vector boson (and ghost) mass matrix is  $m_V^2 = \mathcal{D}_1(\mathcal{D}_1)^T + \mathcal{D}_2(\mathcal{D}_2)^T$ , the Goldstones mass matrix is:

$$m_v^2 = (\mathcal{D}_1)^T \mathcal{D}_1 + (\mathcal{D}_2)^T \mathcal{D}_2, \quad (\text{A3})$$

therefore we get

$$m_v^2 = \frac{v^2}{4} \begin{pmatrix} g^2 & 0 & 0 \\ 0 & g^2 & 0 \\ 0 & 0 & g^2 + g_1^2 \end{pmatrix}. \quad (\text{A4})$$

The mass matrix in Equation (A4) shows that the Goldstones have a mass that is equivalent to the SM-ones, as expected since the gauge sector has not been extended.

As we have already intimated, the ghost mass matrix and interactions are defined by means of the same matrix  $\mathcal{D}$  via

$$m_{ghost}^2 = \mathcal{D}_1(\mathcal{D}_1)^T + \mathcal{D}_2(\mathcal{D}_2)^T. \quad (\text{A5})$$

Notice that the  $m_{ghost}^2$  and the  $m_v^2$  of equation (A4) have different numbers of zero-eigenvalues, but their non-zero eigenvalues are in a one-to-one correspondence; furthermore, the eigenvalues of the gauge-fixing mass matrix are the same of the gauge boson mass matrix, as expected.

Then, the ghost Lagrangian is defined as

$$\begin{aligned} \mathcal{L}_{ghost} = & -\bar{c}^a \left[ (\partial_\mu D^\mu)^{ab} + \mathcal{D}_1^a \cdot (\mathcal{D}_1^b + \mathcal{S}_1^b)^T \right] c^b \\ & - \bar{c}^a \left[ \mathcal{D}_2^a \cdot (\mathcal{D}_2^b + \mathcal{S}_2^b)^T \right] c^b, \end{aligned} \quad (\text{A6})$$

---

<sup>3</sup> The  $4 \times 3$  matrix follows from the four gauge bosons  $W^i|_{i=1,3}$ ,  $Z$ , and the three Goldstone bosons  $\phi^i|_{i=1,3}$ .

where the matrices  $\mathcal{S}_{1,2}$  represent the link between the fluctuations (Goldstones) of the Higgses around their VEVs and the gauge bosons; a convenient<sup>4</sup> way to write this matrices is

$$(\mathcal{S}_1)^T = \frac{1}{2} \begin{pmatrix} g\eta_1 & c_\beta g z & -c_\beta g w_2 & -c_\beta g_1 w_2 \\ -c_\beta g z & g\eta_1 & c_\beta g w_1 & c_\beta g_1 w_1 \\ c_\beta g w_2 & -c_\beta g w_1 & g\eta_1 & -g_1 \eta_1 \end{pmatrix}, \quad (\text{A7})$$

$$(\mathcal{S}_2)^T = \frac{1}{2} \begin{pmatrix} g\eta_2 & s_\beta g z & -s_\beta g w_2 & -s_\beta g_1 w_2 \\ -s_\beta g z & g\eta_2 & s_\beta g w_1 & s_\beta g_1 w_1 \\ s_\beta g w_2 & -s_\beta g w_1 & g\eta_2 & -g_1 \eta_2 \end{pmatrix}, \quad (\text{A8})$$

where

$$w_1 = \frac{w^+ + w^-}{\sqrt{2}}, \quad (\text{A9})$$

$$w_2 = i \frac{w^+ - w^-}{\sqrt{2}}. \quad (\text{A10})$$

Finally, the ghost fields  $(\bar{c})$  read as

$$c = \begin{pmatrix} w_1^g & w_2^g & w_3^g & B^g \end{pmatrix}, \quad (\text{A11})$$

where

$$w_1^g = \frac{w_g^+ + w_g^-}{\sqrt{2}}, \quad (\text{A12})$$

$$w_2^g = i \frac{w_g^+ - w_g^-}{\sqrt{2}}, \quad (\text{A13})$$

$$w_3^g = \cos \theta_W z_g + \sin \theta_W A_g, \quad (\text{A14})$$

$$B^g = -\sin \theta_W z_g + \cos \theta_W A_g. \quad (\text{A15})$$

## Appendix B: Perturbativity at high $\tan\beta$

In order to properly realise the high  $\tan\beta$  scenario, we must carefully consider the perturbativity of the couplings. Firstly, from Equation (12) we see that the  $\tan\beta \rightarrow \infty$  approximation leads to the following definition of the heaviest neutral scalar mass:

$$M_3^2 = - \sum_{i=1}^2 M_i^2 \frac{R_{i2} R_{i3}}{R_{32} R_{33}}. \quad (\text{B1})$$

From Equations (17) we can conclude that all the couplings are finite and perturbatively small except for  $\lambda_1$  and  $\lambda_3$ .<sup>5</sup> In fact, for  $\tan\beta \rightarrow \infty$  or equivalently  $\cos\beta \rightarrow 0$  and  $\sin\beta \rightarrow 1$ ,

<sup>4</sup> In fact, the explicit calculation of each single matrix gives rise to connection between ghosts and both the charged Higgses and the  $\eta_3$  combination of scalar fields. Consistently, the sum of the two contributions disarms these connections: ghost fields do not link to charged Higgs.

<sup>5</sup> While also  $\text{Im}\lambda_5$  is apparently divergent, by plugging the definition of  $M_3^2(\tan\beta \rightarrow \infty)$  in (17f) it is easy to see that the result is always finite. If  $v_1$  exactly vanishes, one can rotate away the phase of  $\lambda_5$  to render  $CP$ -conservation manifest [56].

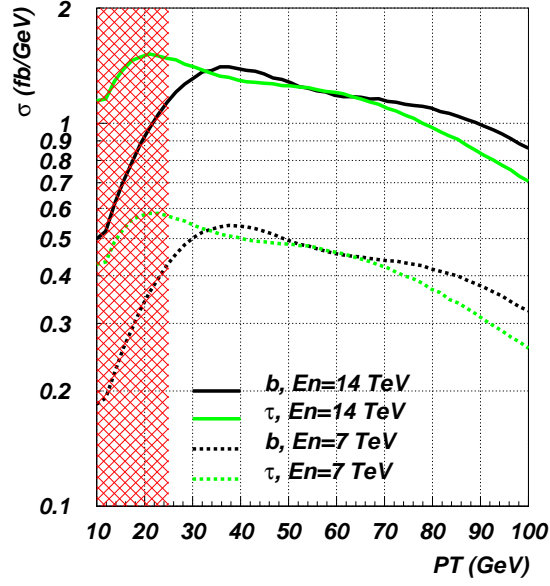


FIG. 8. Differential cross-sections of the process  $pp \rightarrow W \rightarrow H^\pm H_1 \rightarrow \tau^\pm \nu b \bar{b}$  with respect to  $p_T$  of the  $b$ -quark and the  $\tau$ -lepton at the indicated centre-of-mass energies, for the benchmark point  $P_1$ . Each curve is the sum of  $d\sigma(pp \rightarrow \tau^\pm \nu b \bar{b})/dp_T$  and that for the conjugate final state. The shadowed range (red online) shows the selection cuts set for the signal-to-background analysis.

the two potentially diverging couplings become:

$$\lambda_1 \simeq \frac{1}{v^2 \cos^2 \beta} \left[ -\mu^2 + \sum M_i^2 \left( R_{i1}^2 - \frac{R_{i2} R_{i3} R_{31}^2}{R_{32} R_{33}} \right) \right], \quad (\text{B2})$$

$$\lambda_3 \simeq \frac{M_1^2 - M_2^2}{v^2 \cos \beta} \frac{R_{22} R_{12}}{R_{33}}. \quad (\text{B3})$$

Hence, no matter how large  $\tan \beta$  is, we can always keep  $\lambda_1$  and  $\lambda_3$  perturbatively small by choosing

$$\mu^2 \simeq \sum M_i^2 \left( R_{i1}^2 - \frac{R_{i2} R_{i3} R_{31}^2}{R_{32} R_{33}} \right), \quad (\text{B4})$$

$$M_1 \simeq M_2, \quad (\text{B5})$$

respectively. This shows that there is no strict upper limit on  $\tan \beta$  from perturbativity. However, we do not make use of this mechanism for drawing our conclusions in the main part of the present paper.

### Appendix C: $p_T$ distributions of $b$ and $\tau$

In figure 8, we show the  $p_T$  spectra for the  $b$ -quark and the  $\tau$ -lepton, extracted from the process  $pp \rightarrow W \rightarrow H^\pm H_1 \rightarrow \tau^\pm \nu b \bar{b}$  at the LHC. They were evaluated at the benchmark point  $P_1$ . In the  $p_{T,b}$  distributions, one finds that the selection cuts in (25) act on regions with suppressed differential cross-sections. This means that we retain the major portion



of events at our disposal even after applying the cuts. Even in the  $p_{T,\tau}$  distributions, the excluded area below each curve is relatively small compared to the total cross-section.

- 
- [1] S. Weinberg, *Gauge hierarchies*, *Phys. Lett.* **B82** (1979) 387; M. Veltman, *The infrared-ultraviolet connection*, *Acta Phys. Polon.* **B12** (1981) 437; C. H. Llewellyn Smith and G. G. Ross, *The real gauge hierarchy problem*, *Phys. Lett.* **B105** (1981) 38.
  - [2] P. Fayet, *Supersymmetry and weak, electromagnetic and strong interactions*, *Phys. Lett.* **B64** (1976) 159.
  - [3] T. D. Lee, *A theory of spontaneous T violation*, *Phys. Rev.* **D8** (1973) 1226; *CP nonconservation and spontaneous symmetry breaking*, *Phys. Rept.* **9** (1974) 143.
  - [4] S. Weinberg, *Gauge theory of CP violation*, *Phys. Rev. Lett.* **37** (1976) 657.
  - [5] See e.g. J. L. Rosner, *An  $E_6$  interpretation of an  $e^+e^-\gamma\gamma \not{E}_T$  event*, *Phys. Rev.* **D55** (1997) 3143 [hep-ph/9607467]; S. King, S. Moretti, and R. Nevzorov, *Exceptional supersymmetric standard model*, *Phys. Lett.* **B634** (2006) 278, [hep-ph/0511256].
  - [6] See e.g. L. Basso, S. Moretti, and G. M. Pruna, *Theoretical constraints on the couplings of non-exotic minimal  $Z'$  bosons*, *JHEP* **1108** (2011) 122, [arXiv:1106.4762].
  - [7] R. Peccei and H. R. Quinn, *Constraints imposed by CP conservation in the presence of instantons*, *Phys. Rev.* **D16** (1977) 1791.
  - [8] See e.g. I. Antoniadis, E. Kiritsis, and T. Tomaras, *A D-brane alternative to unification*, *Phys. Lett.* **B486** (2000) 186, [hep-ph/0004214].
  - [9] See e.g. M. Gonderinger, Y. Li, H. Patel, and M. J. Ramsey-Musolf, *Vacuum stability, perturbativity, and scalar singlet dark matter*, *JHEP* **01** (2010) 053, [arXiv:0910.3167].
  - [10] H. Haber, G. L. Kane, and T. Sterling, *The fermion mass scale and possible effects of Higgs bosons on experimental observables*, *Nucl. Phys.* **B161** (1979) 493.
  - [11] See e.g. K. S. Babu and J. Kubo, *Dihedral families of quarks, leptons and Higgses*, *Phys. Rev.* **D71** (2005) 056006, [hep-ph/0411226].
  - [12] See e.g. E. Ma, *Naturally small seesaw neutrino mass with no new physics beyond the TeV scale*, *Phys. Rev. Lett.* **86** (2001) 2502–2504, [hep-ph/0011121]; S. M. Davidson and H. E. Logan, *Dirac neutrinos from a second Higgs doublet*, *Phys. Rev.* **D80** (2009) 095008, [arXiv:0906.3335].
  - [13] N. G. Deshpande and E. Ma, *Pattern of symmetry breaking with two Higgs doublets*, *Phys. Rev.* **D18** (1978) 2574.
  - [14] R. Barbieri, L. J. Hall, and V. S. Rychkov, *Improved naturalness with a heavy Higgs: An alternative road to LHC physics*, *Phys. Rev.* **D74** (2006) 015007, [hep-ph/0603188]; M. Gustafsson, E. Lundstrom, L. Bergstrom, and J. Edsjo, *Significant gamma lines from inert Higgs dark matter*, *Phys. Rev. Lett.* **99** (2007) 041301, [astro-ph/0703512].
  - [15] See e.g. H.-S. Goh, L. J. Hall, and P. Kumar, *The leptonic Higgs as a messenger of dark matter*, *JHEP* **0905** (2009) 097, [arXiv:0902.0814].
  - [16] See e.g. N. Turok and J. Zadrozny, *Electroweak baryogenesis in the two doublet model*, *Nucl. Phys.* **B358** (1991) 471.
  - [17] See e.g. J.-O. Gong, H. M. Lee, and S. K. Kang, *Inflation and dark matter in two Higgs doublet models*, arXiv:1202.0288.
  - [18] See e.g. R. Schabinger and J. D. Wells, *A minimal spontaneously broken hidden sector and its impact on Higgs boson physics at the Large Hadron Collider*, *Phys. Rev.* **D72** (2005) 093007,



- [hep-ph/0509209].
- [19] K.-m. Cheung, C.-H. Chou, and O. C. Kong, *Muon anomalous magnetic moment, two Higgs doublet model, and supersymmetry*, *Phys. Rev.* **D64** (2001) 111301, [hep-ph/0103183].
  - [20] A. J. Buras, M. V. Carlucci, S. Gori, and G. Isidori, *Higgs-mediated FCNCs: natural flavour conservation vs. minimal flavour violation*, *JHEP* **1010** (2010) 009, [arXiv:1005.5310].
  - [21] J.-h. Park, *Lepton non-universality at LEP and charged Higgs*, *JHEP* **0610** (2006) 077, [hep-ph/0607280].
  - [22] P. Ko, Y. Omura, and C. Yu, *Chiral U(1) flavor models and flavored Higgs doublets: the top FB asymmetry and the  $Wjj$* , *JHEP* **1201** (2012) 147, [arXiv:1108.4005].
  - [23] ATLAS Collaboration, G. Aad *et al.*, *Search for the Standard Model Higgs boson in the diphoton decay channel with  $4.9 \text{ fb}^{-1}$  of  $pp$  collisions at  $\sqrt{s} = 7 \text{ TeV}$  with ATLAS*, *Phys. Rev. Lett.* **108** (2012) 111803, [arXiv:1202.1414].
  - [24] CMS Collaboration, S. Chatrchyan *et al.*, *Search for the Standard Model Higgs boson decaying into two photons in  $pp$  collisions at  $\sqrt{s} = 7 \text{ TeV}$* , arXiv:1202.1487.
  - [25] ATLAS Collaboration, G. Aad *et al.*, *Combined search for the Standard Model Higgs boson using up to  $4.9 \text{ fb}^{-1}$  of  $pp$  collision data at  $\sqrt{s} = 7 \text{ TeV}$  with the ATLAS detector at the LHC*, *Phys. Lett.* **B710** (2012) 49, [arXiv:1202.1408].
  - [26] CMS Collaboration, S. Chatrchyan *et al.*, *Combined results of searches for the Standard Model Higgs boson in  $pp$  collisions at  $\sqrt{s} = 7 \text{ TeV}$* , arXiv:1202.1488.
  - [27] ALEPH Collaboration, DELPHI Collaboration, L3 Collaboration, OPAL Collaboration, LEP Electroweak Working Group, J. Alcaraz *et al.*, *A combination of preliminary electroweak measurements and constraints on the Standard Model*, hep-ex/0612034.
  - [28] R. Dermisek, *Light charged Higgs and lepton universality in  $W$  boson decays*, arXiv:0807.2135; R. Dermisek, *Light charged and CP-odd Higgses in MSSM-like models*, *AIP Conf. Proc.* **1078** (2009) 226, [arXiv:0809.3545]; K. J. Bae, R. Dermisek, D. Kim, H. D. Kim, and J.-H. Kim, *Light Higgs scenario in BMSSM and LEP precision data*, arXiv:1001.0623.
  - [29] A. Filipuzzi, J. Portoles, and M. Gonzalez-Alonso,  *$U(2)^5$  flavor symmetry and lepton universality violation in  $W \rightarrow \tau \nu_\tau$* , arXiv:1203.2092.
  - [30] See e.g. V. D. Barger, J. Hewett, and R. Phillips, *New constraints on the charged Higgs sector in two Higgs doublet models*, *Phys. Rev.* **D41** (1990) 3421.
  - [31] A. Pilaftsis and C. E. M. Wagner, *Higgs bosons in the minimal supersymmetric standard model with explicit CP violation*, *Nucl. Phys.* **B553** (1999) 3, [hep-ph/9902371].
  - [32] S. L. Glashow and S. Weinberg, *Natural conservation laws for neutral currents*, *Phys. Rev.* **D15** (1977) 1958.
  - [33] A. W. El Kaffas, W. Khater, O. M. Ogreid, and P. Osland, *Consistency of the two Higgs doublet model and CP violation in top production at the LHC*, *Nucl. Phys.* **B775** (2007) 45, [hep-ph/0605142].
  - [34] W. Khater and P. Osland, *CP violation in top quark production at the LHC and two Higgs doublet models*, *Nucl. Phys.* **B661** (2003) 209, [hep-ph/0302004].
  - [35] I. Ginzburg and I. Ivanov, *Tree-level unitarity constraints in the most general 2HDM*, *Phys. Rev.* **D72** (2005) 115010, [hep-ph/0508020].
  - [36] See e.g. S. Kanemura, Y. Okada, E. Senaha, and C.-P. Yuan, *Higgs coupling constants as a probe of new physics*, *Phys. Rev.* **D70** (2004) 115002, [hep-ph/0408364].
  - [37] OPAL Collaboration, G. Abbiendi *et al.*, *Search for charged Higgs bosons in  $e^+e^-$  collisions at  $\sqrt{s} = 189\text{--}209 \text{ GeV}$* , *Eur. Phys. J.* **C72** (2012) 2076, [arXiv:0812.0267].

- [38] ATLAS Collaboration, *An update to the combined search for the Standard Model Higgs boson with the ATLAS detector at the LHC using up to  $4.9 \text{ fb}^{-1}$  of pp collision data at  $\sqrt{s} = 7 \text{ TeV}$* , ATLAS-CONF-2012-019; CMS Collaboration, M. Pieri *et al.*, *Searches for the Standard Model Higgs Boson at CMS*, arXiv:1205.2907.
- [39] H. E. Haber and H. E. Logan, *Radiative corrections to the  $Zb\bar{b}$  vertex and constraints on extended Higgs sectors*, *Phys. Rev.* **D62**, 015011 (2000) [hep-ph/9909335].
- [40] D. Toussaint, *Renormalization effects from superheavy Higgs particles*, *Phys. Rev.* **D18**, 1626 (1978); S. Bertolini, *Quantum effects in a two Higgs doublet model of the electroweak interactions*, *Nucl. Phys.* **B272**, 77 (1986); W. Hollik, *Nonstandard Higgs bosons in  $SU(2) \times U(1)$  radiative corrections*, *Z. Phys.* **C32**, 291 (1986); *Radiative corrections with two Higgs doublets at LEP / SLC and HERA*, *Z. Phys.* **C37**, 569 (1988).
- [41] ATLAS Collaboration, G. Aad *et al.*, *Search for charged Higgs bosons decaying via  $H^+ \rightarrow \tau\nu$  in top quark pair events using pp collision data at  $\sqrt{s} = 7 \text{ TeV}$  with the ATLAS detector*, arXiv:1204.2760; CMS Collaboration, S. Chatrchyan *et al.*, *Search for a light charged Higgs boson in top quark decays in pp collisions at  $\sqrt{s} = 7 \text{ TeV}$* , arXiv:1205.5736.
- [42] J. L. Diaz-Cruz and O. A. Sampayo, *Contribution of gluon fusion to the production of charged Higgs at hadron colliders*, *Phys. Rev.* **D50** (1994) 6820.
- [43] A. Djouadi, W. Kilian, M. Muhlleitner, and P. Zerwas, *Production of neutral Higgs boson pairs at LHC*, *Eur. Phys. J.* **C10** (1999) 45, [hep-ph/9904287].
- [44] A. G. Akeroyd and M. A. Diaz, *Searching for a light fermiophobic Higgs boson at the Tevatron*, *Phys. Rev.* **D67** (2003) 095007, [hep-ph/0301203]; A. Akeroyd, M. A. Diaz, and F. J. Pacheco, *Double fermiophobic Higgs boson production at the CERN LHC and LC*, *Phys. Rev.* **D70** (2004) 075002, [hep-ph/0312231].
- [45] I. F. Ginzburg, *Light charged Higgs at LHC*, arXiv:1205.5890.
- [46] A. V. Semenov, *LanHEP: A package for automatic generation of Feynman rules in gauge models*, hep-ph/9608488.
- [47] A. Pukhov, *CalcHEP 2.3: MSSM, structure functions, event generation, batchs, and generation of matrix elements for other packages*, hep-ph/0412191; <http://theory.sinp.msu.ru/pukhov/calchep.html>.
- [48] P. M. Nadolsky, H.-L. Lai, Q.-H. Cao, J. Huston, J. Pumplin, D. Stump, W.-K. Tung and C.-P. Yuan, *Implications of CTEQ global analysis for collider observables*, *Phys. Rev.* **D78** (2008) 013004 [arXiv:0802.0007].
- [49] T. Hahn and M. Perez-Victoria, *Automatized one loop calculations in four-dimensions and D-dimensions*, *Comput. Phys. Commun.* **118** (1999) 153, [hep-ph/9807565].
- [50] S. I. Bityukov and N. V. Krasnikov, *On the observability of a signal above background*, *Nucl. Instrum. Meth.* **A452** (2000) 518; S. Bityukov, S. Erofeeva, N. Krasnikov, and A. Nikitenko, *Program for evaluation of significance, confidence intervals and limits by direct calculation of probabilities*, in *Statistical problems in particle physics, astrophysics and cosmology: Proceedings of PHYSTAT05, Oxford, UK, 12–15 Sep 2005* (L. Lyons and M. K. Ünel, eds.), pp. 106–107, Imperial College Press, 2005.
- [51] TEVNPH (Tevatron New Phenomina and Higgs Working Group), CDF Collaboration, D0 Collaboration, *Combined CDF and D0 search for Standard Model Higgs boson production with up to  $10.0 \text{ fb}^{-1}$  of data*, arXiv:1203.3774.
- [52] N. Bernal, D. Lopez-Val, and J. Sola, *Single Higgs-boson production through  $\gamma\gamma$  scattering within the general 2HDM*, *Phys. Lett.* **B677** (2009) 39, [arXiv:0903.4978]; D. Lopez-Val and J. Sola, *Single Higgs-boson production at a photon-photon collider: general 2HDM versus*

- MSSM*, *Phys. Lett.* **B702** (2011) 246, [arXiv:1106.3226].
- [53] P. Posch, *Enhancement of  $h \rightarrow \gamma\gamma$  in the two Higgs doublet model type I*, *Phys. Lett.* **B696** (2011) 447, [arXiv:1001.1759].
  - [54] A. Arhrib, R. Benbrik, and N. Gaur,  *$H \rightarrow \gamma\gamma$  in inert Higgs doublet model*, arXiv:1201.2644.
  - [55] M. E. Peskin and D. V. Schroeder, *An introduction to quantum field theory*, Addison-Wesley, 1995.
  - [56] I. F. Ginzburg and M. Krawczyk, *Symmetries of two Higgs doublet model and  $CP$  violation*, *Phys. Rev.* **D72** (2005) 115013, [hep-ph/0408011].